Surface & Coatings Technology 328 (2017) 231–239

Contents lists available at ScienceDirect

Surface & Coatings Technology

journal homepage: www.elsevier.com/locate/surfcoat

Microreactor with copper oxide nanostructured films for catalytic gas phase oxidations

Rocío L. Papurello, Ana P. Cabello, María A. Ulla, Claudia A. Neyertz, Juan M. Zamaro *

Instituto de Investigaciones en Catálisis y Petroquímica, INCAPE (FIQ, UNL, CONICET), Santiago del Estero 2829, 3000 Santa Fe, Argentina

ARTICLE INFO

Article history:
Received 13 May 2017
Revised 26 August 2017
Accepted in revised form 29 August 2017
Available online 31 August 2017

Keywords:
CuO_x nanostructures
Microchannel
In-situ growth
Microreactor
Catalysis
CO oxidation

ABSTRACT

Three simple gas phase based methods were applied to copper foils with parallel microchannels to induce in-situ growth of nanostructured CuO_x films. One method consisted in treating with vapors of NH_4OH and H_2O_2 (VAP); another method consisted in heating in air at 500 °C (CAL); and the third one was a sequence of both methods (CAL-VAP). The synthesized CuO_x films/Cu foils were assembled as microreactors and tested for CO oxidation, showing high catalytic performance and stability in reaction. The physicochemical characteristics of the films were examined by Scanning Electron Microscopy (SEM), Temperature-Programmed Reduction (TPR), X-ray Diffraction (XRD), Laser Raman Spectroscopy (LRS), Reflectance Infrared Fourier Transformed Spectroscopy (DRIFTS) and ultrasound tests. The VAP films consisted of thick clustered nanorods containing Cu^+ and Cu^{2+} species in the outer layer of the coating. The CAL films presented uniform growth of nanoneedles in which the outer layers were composed mainly of Cu^{2+}. However, by submitting the CAL sample to the VAP procedure (CAL-VAP), part of CuO was reduced to Cu_4O_3 species. The developed microreactors with copper oxide nanostructures directly grown on microchannels with high thermal conductivity represent a low-cost, simple alternative for application in catalytic gas-phase reactions.

1. Introduction

In recent years, research on catalysts based on copper oxides (CuO_x) has significantly increased since these solids have catalytic activity in numerous oxidation reactions such as CO oxidation [1–3] and have a lower cost than other catalytic formulations involving noble metals. The nanostructured phases of such materials are interesting catalytic solids since they can provide a high active surface with multiple oxidation states. In addition, it has been shown that their efficiency can be maximized if they are arranged as highly dispersed nanoparticles on the surface of microstructured catalysts, also called microreactors [4–6]. These latter ones consist of three-dimensional structures with fluid passages of sub-millimeter dimensions, in whose walls a catalytic material is deposited. They allow an advantageous catalytic performance in comparison with the conventional packed-bed powder catalysts because of the high mass and heat transfer rates they provide [7,8]. On the other hand, when the aim is to carry out highly endo or exothermic reactions, it is convenient to use metallic substrates, which allow obtaining thin walls with high thermal conductivity that facilitate the heat exchange with the catalytic film [9]. In this context, there emerges an interest in studying the growth of CuO_x nanocrystals dispersed on the surface of metallic structures, with the intention of developing new microreactors.

The synthesis of copper oxide films over copper substrates is an interesting option since they can be obtained from the oxidation of the substrate itself. Among the alternatives for obtaining such films, solution-based methods involving hydrothermal treatments are considered a good option. By applying these techniques, CuO growths with nanoflower morphology have been obtained using highly alkaline solutions containing $(NH_4)_2S_2O_8$ [10] or with surfactant-assisted treatments employing sodium dodecyl sulfate (SDS) [11]. In addition, different dimensionalities and architectures of CuO nanocrystals have been achieved by adding other surfactants such as cetyltrimethylammonium (CTAB) or Tx-100 [12] to the alkaline solution. Another strategy that may be advantageous for coating substrates with complex geometries is to use gas phase treatments. Recent studies report the growth of CuO nanowires on substrates with different geometries, such as grids, foils, wires and monoliths, by direct heating of the substrates in air atmosphere [13–18]. On the other hand, a low temperature oxidation method using ammonia and hydrogen peroxide vapors has also been used to obtain CuO nanoribbons [19]. Nanostructured CuO_x films have been employed for example in H_2O_2 peroxide detection [10], electrodes for lithium ion batteries [11,12], NH_3 sensing [13] and electrocatalytic glucose oxidation [19]. To the best of our knowledge, the application of this type of films in microreactors for a gas-solid catalytic reaction has not been reported.

* Corresponding author at: Santiago del Estero 2829, 3000 Santa Fe, Argentina.
E-mail address: zamaro@fiq.unl.edu.ar (J.M. Zamaro).

http://dx.doi.org/10.1016/j.surfcoat.2017.08.066
0257-8972/

We have recently optimized the gas phase treatments discussed above, obtaining homogeneous and densely packed copper oxide nanostructures on the surface of flat copper foils [20]. Based on these studies, in the present work we analyze the in-situ growth of nanostructured CuO_x films on copper substrates with microchannels, which are then evaluated in a microreactor module for the catalytic oxidation of CO as a reaction test.

2. Experimental

2.1. Coating synthesis

Electrolytic copper foils (99.9%, 100 μm thickness) in pieces of 2 × 2.5 cm were used. Microchannels were molded (Fig. 1a) by a home-made device consisting of two micrometric metal rollers whose spacing allows regulating the folding conditions. In this way, copper foils with parallel microchannels which had a hydraulic diameter of about 200 μm and good uniformity in size were obtained (Fig. 1b). The initial mass of the microchannel substrates was similar in all samples and about of 532.5 ± 2 mg. After folding the foils, they were washed with 2 N HCl during 15 min and then with distilled water in ultrasonic bath for 10 min after which the oxidation treatments were applied. Briefly, one method (VAP) consisted in placing the foils suspended vertically above the liquid level in a flask containing a mixture of 10 mL of NH_4OH (Cicarelli, pro-analysis, 37% w/w) and 10 mL of H_2O_2 (Cicarelli, pro-analysis 100 vol.) and heating at 80 °C for 8 h. The other treatment (CAL) consisted in heating the foils vertically supported in static air at 500 °C (2 °C min^{-1}) for 8 h. In addition, a sequential combination was carried out applying first a CAL treatment followed by a VAP treatment (CAL-VAP). The syntheses by these methods were performed under conditions we previously optimized with flat copper foils in which the best morphological characteristics of the oxide layers were obtained [20].

2.2. Sample characterization

The microstructure of the oxide films was examined by Scanning Electron Microscopy (SEM) with a JEOL JSM-35C operated at 20 kV. The samples were glued to the sample holder with Ag painting and then coated with a thin layer of Au in order to improve the images. Diffuse Reflectance Fourier Transformed Spectroscopy (DRIFTS) was performed with a Shimadzu Prestige instrument (accumulation 40 scans, resolution 2 cm^{-1}) equipped with a MCT detector. X-ray Diffraction (XRD) was performed with a Shimadzu XD-D1 instrument by scanning the 2θ angle at 2° min^{-1} between 30° and 55° using CuKα radiation (λ = 1.5418 Å, 30 kV, 40 mA). The mechanical stability of the films was evaluated subjecting the samples to a test consisting in an ultrasound treatment. The samples were immersed in a solvent (water or acetone) inside a glass vessel and then in an ultrasonic bath (Cole-Parmer, 47 kHz and 130 W) at 30 °C for different periods. After that, the samples were dried at 120 °C during 10 min and the weight were measured both before and after the treatment with a microbalance Mettler Toledo MT5 (0.001 mg accuracy). The reducibility of the films was analyzed by Temperature-Programmed Reduction with Hydrogen (H_2-TPR) in a Micromeritics Autochem II equipment. First a pretreatment in Ar was carried out (200 °C, 1 h) and then the TPR was performed in a H_2 (5%)/Ar stream with a ramp of 10 °C/min up to 900 °C. Laser Raman Spectroscopy (LRS) was performed on microreactors using a LabRam spectrometer (Horiba–Jobin–Yvon) coupled to an Olympus confocal microscope equipped with a CCD detector cooled to about 200 K. The excitation wavelength was 532 nm (Spectra Physics argon-ion laser) and the laser power was set at 30 mW.

2.3. Catalytic evaluations in a microreactor

The substrates with the oxide coatings were stacked inside a microreactor module, placing two units between a flat steel plate in such a way that the microreactor was made up of 108 parallel microchannels. The module was connected to a continuous flow system equipped with flow mass controllers (Brooks 4800) and it was heated by heating cartridges controlled with a PID control system by means of a thermocouple inserted in the housing under the surface of the catalytic foils. Prior to the catalytic evaluation, the microreactors were heated in He (30 mL min^{-1}) between room temperature and 300 °C (5 °C min^{-1}) and maintained at that temperature for 30 min. After that, the catalytic runs were performed using a molar gas feed composition of 1% CO, 2% O_2 in He balance employing a total gas flow of 30 cm^3 min^{-1}. The catalytic measurements were performed after stabilizing the microreactors at different temperatures in heating and cooling ramps and the stability in reaction was also analyzed by keeping the microreactors under reaction at a given temperature for long periods. The CO conversions were determined by analyzing the microreactor exit with an on-line Shimadzu GC-2014 chromatograph equipped with a TCD detector and a 5A molecular sieve column. CO conversions were calculated as: $X_{CO} = ([CO]° - [CO]) / [CO]°$; where X is conversion, $[CO]°$ and [CO] are inlet and outlet gas concentrations.

3. Results and discussion

3.1. Growth of nanostructured CuO_x films on microchannels

After subjecting the substrates to the CAL, VAP or CAL-VAP treatments, respectively, a weight gain similar for the three samples (CAL: 9 mg, VAP: 9.4 mg, CAL-VAP: 12.4 mg) was recorded, which corresponds to a mass of oxygen gained during the oxidation of the substrates. The surface of these samples turned black indicating the

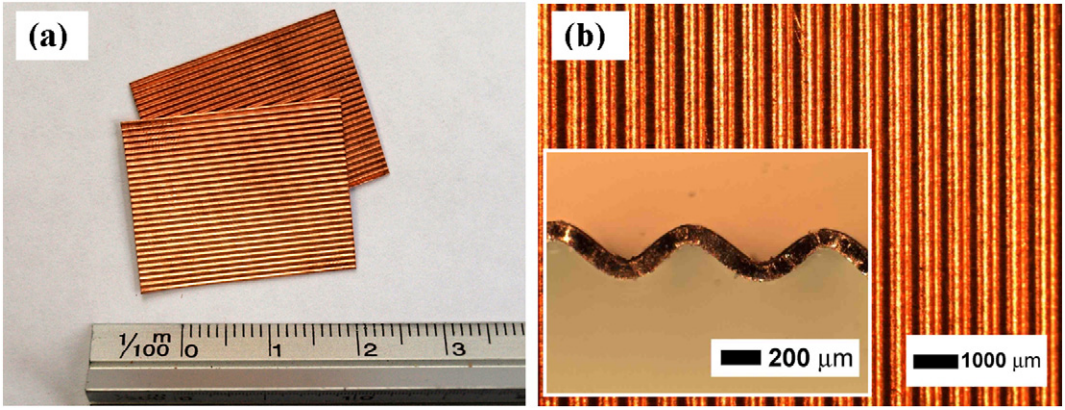

Fig. 1. Optical micrographs of the as-prepared substrate: a) microchanneled foils; b) close-view of microchannels.

formation of oxide layers which was confirmed by XRD, indicating a mixture of CuO and Cu_2O phases (shown below). The analysis of these films by TPR (Fig. 2) showed for the CAL sample a symmetric signal centered around 360 °C, while for the VAP sample the profile was asymmetric and displaced towards the lower temperature zone. Meanwhile, CAL-VAP sample presented a profile similar to CAL but with a contribution at low temperatures, showing the combined nature of this film. The signals at lower temperature can be assigned to both small size CuO crystals similar to those found for supported CuO nanoparticles [6,21] and also to Cu_2O nanocrystals that show low reduction temperatures [22]. The total hydrogen consumption with respect to the mass of oxygen gained (H_2/O in mmol/mg) exhibited similar values for the three cases (CAL: 5.03 10^{-2}, VAP: 5.17 10^{-2}, CAL-VAP: 4.95 10^{-2}). These consumptions, in turn, were lower than those corresponding to the CuO powder (6.24 10^{-2}) in line with the fact that the films were a mixture of Cu^{+} and Cu^{2+} oxides. Through the H_2/O ratios a Cu^{2+} proportion as CuO was estimated, being 76 wt% for CAL, 78 wt% for VAP and 74 wt% for CAL-VAP films, respectively.

The SEM image of the VAP sample indicates a total coverage of the microchannel surface (Fig. 3a) with homogeneous arrangements of structures in the form of thickly clustered nanorods of about 1 μm length and 150 nm width at the end of the rods on the film surface. In some sectors they are grouped in formations with a chrysanthemum-like architecture. The overall thickness of these VAP films is about 13 μm (Fig. 3b). On the other hand, the CAL sample presents a uniform growth of nanoneedles that cover homogeneously the surface of the microchannels (Fig. 3c). By the CAL method, a layered growth is produced with a base of Cu_2O on which a CuO film is developed, from which CuO nanoneedles grow (Fig. 3d). The cross section shows a base layer of about 4 μm and CuO nanowires of about 9 μm in length and 260 nm in width. It is interesting to note that the nanoneedles are grouped in the form of islands, which is better visualized in the crests of the microchannels (Fig. 3c). This characteristic is similar to that observed on the surface of flat foils and can be due to surface defects in the bare copper foil which has micrometer size crater-like hollows [20]. The arrangement of the nanostructures in the CAL-VAP film is slightly modified with respect to the CAL sample (Fig. 3e–f). Although the overall thickness of the base film (~5 μm) and the average length of the needles (~9 μm) are maintained, a needles widening (520 nm) as well as a reduction in the amount thereof is observed.

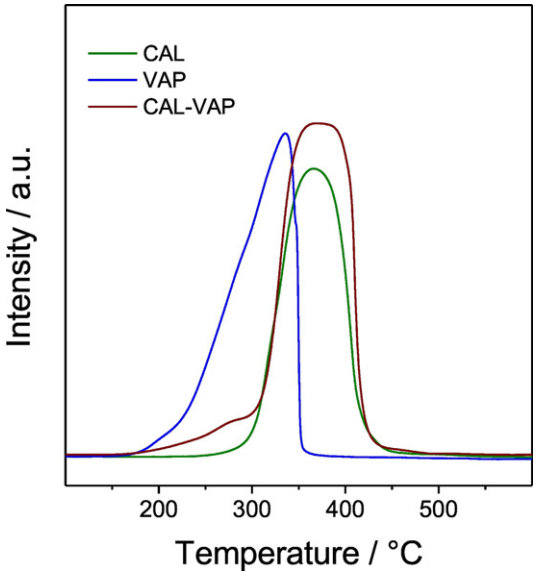

Fig. 2. Hydrogen-Temperature Programmed Reduction (H_2-TPR) of the CuO_x films.

3.2. Mechanical stability of CuO_x films onto microchannels

A crucial aspect for the application of these coatings under real conditions is their mechanical stability. Qualitatively, the three types of films had an acceptable adhesion since there was no severe detachment during their handling and after the cuts made for SEM analysis (see Fig. 3). In order to analyze this property more rigorously, stability tests with ultrasound were performed. In Fig. 4 the results for the coatings subjected to different treatment times using both acetone (Fig. 4a) and water (Fig. 4b) are presented. Initially, a high coating loss is observed which then reaches stabilization. The VAP film grown on plicated foils (VAP/P) presents the highest stability (Fig. 4a), while a CAL treatment followed by VAP (CAL-VAP) remarkably increases the stability of the film with respect to the CAL case. The adhesion order from highest to lowest was: VAP > CAL-VAP > CAL. In order to observe the effect of the microchannel geometry on the coating stability, CAL, VAP and CAL-VAP films grown on flat substrates were also analyzed (empty symbols). A profile and order of stability similar to those discussed above were observed. However, a remarkable increase of the adhesion of the coatings in the foils with microchannels was verified.

In order to better differentiate the stability between coatings, studies in water were performed (Fig. 4b). The mechanism of ultrasonic cavitation involved in these tests depends on the elastic characteristics (surface tension), viscosity and vapor pressure of the liquid medium in any ultrasonic wave [23]. A more severe condition is generated when water is used, given the greater cavitation intensity in this solvent. The cavitation effect results in a high velocity of fluid movement, e.g. microjets, which impacts on the surface of the coating generating its erosion [24]. This test carried out in water (Fig. 4b) allowed us to confirm the order of stability of the coatings, as well as the remarkable increase of the stability of the films grown on microchannels compared to those grown on flat substrates. The question of the origin of this effect was raised and, in principle, two factors could be considered, i) a better distribution of the stresses of the film on the surface with undulated geometry, ii) changes in the surface microstructure of the substrate due to the compression during the folding. To inquire about these possibilities, a sample with microchannels was flattened by compression and then subjected to a CAL treatment. The stability assay of this sample (Fig. 4b) showed a level of film adhesion similar to that of the coating on the flat foil, although the profile was somewhat attenuated at first (Fig. 4b). This result strongly suggests that the increase of the stability of the films on microchannels is fundamentally due to a geometric effect, probably by a better stabilization of the film onto the undulated surface. It should be remarked that the adhesion differences among films were only evident after subjecting the samples to the aggressive ultrasound test, but all coatings were stable under the reaction conditions of the catalytic assays.

3.3. Catalytic performance of nanostructured films in a microreactor

The films were evaluated in a microreactor for the oxidation of carbon monoxide. CO is an extremely toxic gas that accumulates indoors and should be removed [25]; on the other hand it needs to be removed from hydrogen streams used in fuel cells [26] (through the COProx reaction). But also, this is a highly exothermic and simple gas phase oxidation reaction which is suitable to be taken as a model reaction to analyze the behavior of the films. Fig. 5a shows that the three types of coatings were very active. Catalytic performances were analyzed by first increasing the temperature from 30 to 300 °C (Fig. 5a - inc. T) and then, decreasing the temperature from the latter to 30 °C (Fig. 5a - dec. T). The activity trend followed the order CAL < VAP ≈ CAL-VAP, although the CAL-VAP microreactor seemed to have a better conversion over the whole temperature range. We emphasize that no detachments of the three types of films were observed during the catalytic runs. Moreover it should be noted that the Cu microchannel plate without

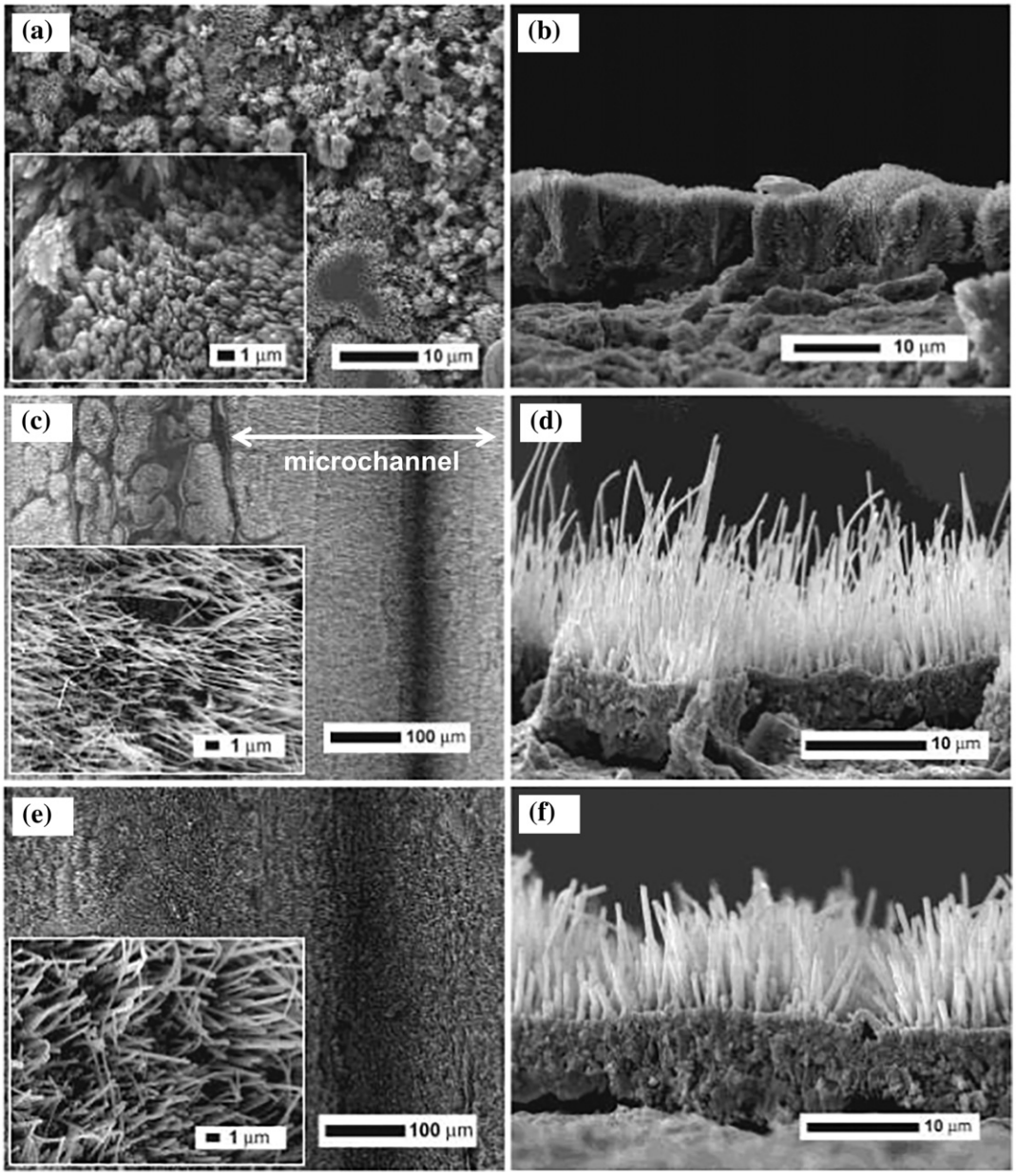

Fig. 3. SEM images of the as synthesized CuO_x films obtained by three different methods: a–b) VAP; c–d) CAL; e–f) CAL-VAP.

CuO_x coatings have a low catalytic activity, reaching a CO conversion of 31% at 300 °C (Fig. 5a).

The high performance of these microreactors can be attributed to two factors: i) the nanostructured nature of the oxide, considering that the CO oxidation reaction on CuO_x nanostructures is influenced by the shape and the exposed plane of the oxide [27], ii) its conformation as a thin film in a microreactor, where a high contact surface is generated between the reactant stream and the catalytic surface, as well as the high mass and heat transfer rates given by the microreactor. The catalytic performance of the CAL film is associated with the needle morphology of CuO that presents selectively exposed (−111) planes with more surface lattice oxygen which can improve the speed of this reaction. The latter follows a Mars-van Krevelen mechanism involving transfer of oxygen from the oxide network through the solid-gas interface and therefore, the reaction rate will be much higher when more oxygen from the network is exposed at the surface [28]. This sample exhibited a T^{50} (temperature at which the CO conversion is 50%) of 190 °C with a X^{175}/O ratio of 1.5 (X^{175} is the CO conversion at 175 °C and O is the weight gain of the evaluated catalytic foils in mg). The latter brings a more precise comparison among films because it takes into account the slight difference in the amount of oxide among them. These results are summarized in Table 1. In addition, a hysteresis loop with a shift towards lower temperatures was observed, which could be due to kinetic effects frequently reported in the literature on CO oxidation with supported metal catalysts [29].

On the other hand, the activity of the VAP and CAL-VAP microreactors (Fig. 5a) was higher than CAL, reaching a total conversion around 225 °C for both cases with a T^{50} of 166 °C and 163 °C, respectively. The X^{175}/O ratios were 3.2, pointing out the similar catalytic performance of both microreactors (Table 1). In these cases, the increased activity is associated with the higher reducibility and lower oxidation state of the surface layer of the film oxide. Comparatively, all of the obtained CuO_x microreactors presented a better catalytic performance than those based on Cu-zeolite films (T^{50} = 320 °C) [30]. The same tendency was observed comparing with the catalytic behavior of powdered mixed oxides, such as $Ce_xSm_{1-x}O_2$ nanoparticle mixed oxides (T^{50} > 400 °C) [31] and nanocomposite dispersed oxides of $Ce_xZr_{1-x}O_2$ (T^{50} > 380 °C) [32]. Besides, the addition of CeO_2 as a promoter could

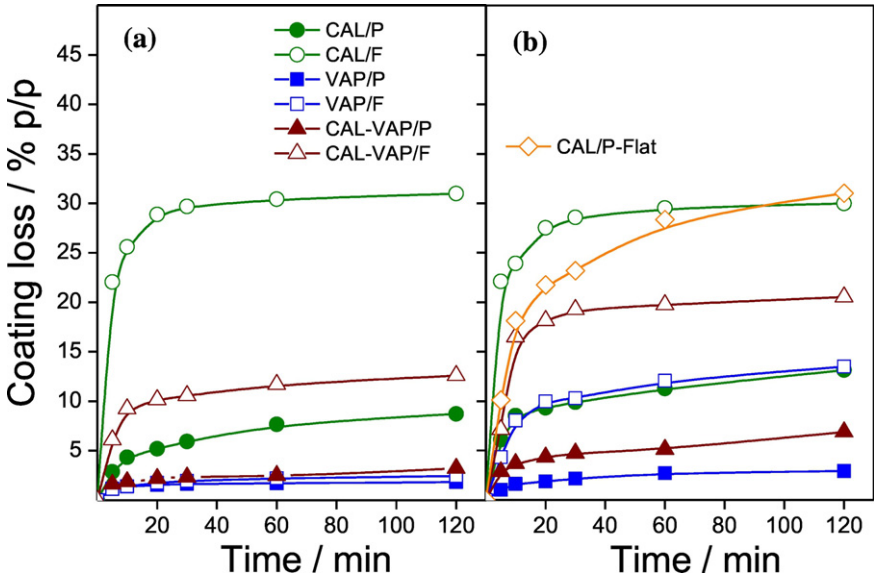

Fig. 4. Mechanical stability of the films: a) employing acetone; b) employing water (P denotes film on plicated foil; F denotes film on flat foil).

further increase the obtained performance, as has been demonstrated in catalysts of $CuOCeO_2$ powder [33] and with a mixture of supported nanoparticles of these phases in a microreactor [6].

Both the activity and the adhesion of the films are fundamental factors for their practical catalytic application. Deciding which is the best catalytic film is always a compromise situation, but in this case our results showed that the film obtained by VAP or CAL-VAP has a better catalytic response and also better adhesion, compared to the CAL sample. However, a third factor should be considered and it is the stability of the films in the reaction stream over time, as discussed below. After the catalytic assays, the microreactors were brought to a conversion level between 70 and 90% and the stability over time in reaction was analyzed. It can be observed (Fig. 5b) that the three coatings were stable in reaction atmosphere for >24 h. For the VAP microreactor a slight initial deactivation was noticed and then stabilized which could be due to a partial sintering of the nanostructures in this sample. It is important to mention that the signals of carbonaceous species (1360 and 1590 cm^{-1}) were absent in the Raman spectra of CuO_x films after being under reaction conditions for >24 h. This evidence is consistent with the fact that the microreactors with nanostructured CuO_x films present a very good catalytic response, being able to maintain a high level of conversion during a long time, which is the main applied objective.

To gain further insight about the CuO_x films properties and their catalytic performance towards the CO oxidation, other physicochemical characterizations were carried out as discussed below.

3.4. Physicochemical characterization of the films

The as synthesized VAP film (fresh sample) developed a mixture of oxides as shown by the diffractogram of Fig. 6. Intense signals corresponding to (111) and (200) planes of Cu_2O phases (JCPDS 5-667), as well as (110), (−111) and (111), (20–2) of the CuO structure (JCPDS 48-1548) can be observed. Additionally, the main signals of Cu^0 from the copper substrate corresponding to the (111) and (200) planes (JCPDS 4-836) are still observed and no signals of other crystalline forms were detected. Likewise, the diffractogram of the CAL sample also indicates the development of a mixture of copper oxides, although

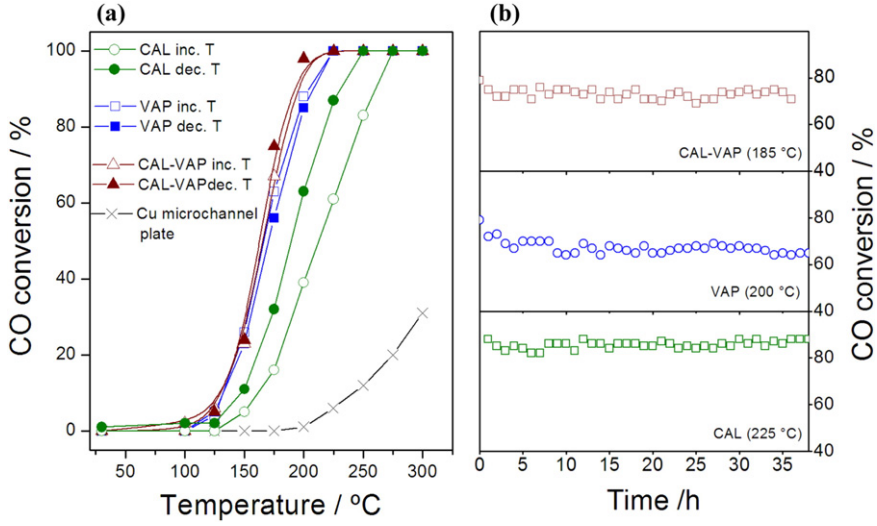

Fig. 5. Catalytic evaluation of CuO_x-based microreactors in CO oxidation: a) Catalytic tests in an increasing temperature program (open symbols) and in a decreasing temperature program (filled symbols); b) Long time stability in reaction.

Table 1
Summary of the catalytic results obtained with the CuO_x-based microreactors.

	CAL	VAP	CAL-VAP
Δm (O), mg	20.6	19.8	23.2
T^{50}, °C	190	166	163
T^{100},°C	250	225	225
X^{175}/Δm (O), %/mg	1.5	3.2	3.2

a more compact layer is suggested given the greater attenuation of the substrate signals. Meanwhile, in the CAL-VAP sample, there were few changes in the XRD pattern compared to the CAL sample. The coatings were characterized after being subjected to the catalytic tests followed by the evaluations of stability in reaction for a long time (used samples). The XRD patterns of the three films (Fig. 6) were similar to those of the fresh samples, indicating that the phase compositions and bulk proportions of the oxides were not modified.

The species identified by Laser Raman Spectroscopy (LRS) on solid materials can be associated with outer-layer compositions in comparison with those obtained by XRD, which are more related to bulk [34]. Therefore, this technique was applied to get more insight about the presence of different copper species. LR spectra of the nanostructured CuO_x coatings, as synthesized and after being under reaction conditions are shown in Fig. 7. The spectrum of the fresh VAP sample presents the characteristic phonon modes of Cu_2O (151, 219, 420, 510 and 630 cm^{-1}) [35–37] and CuO (299, 347 and 630 cm^{-1}) [38,39]. Besides, an important shoulder at 580 cm^{-1} was visualized and it is associated with Cu_4O_3 in agreement with studies by Krüger et al. [39]. This latter phase is not commonly observed in most literature reports because important kinetic factors prevent the formation of Cu_4O_3 as a suboxide or intermediate during the reduction of CuO [40]; (a) O atoms need to be removed from well-defined positions of the CuO lattice, and (b) a substantial distortion (activation energy of about 0.06 eV per atom) in the cell parameters of CuO is required to obtain Cu_4O_3. The most intense XRD reflection of this phase (JPCDS 83–1665) located at $2\theta = 35.7°$ (202) is very close to the most intense signal of CuO at $2\theta = 35.6°$ $(11-1)$ and also to the (111) signal of Cu_2O at $2\theta = 36.4°$. For this

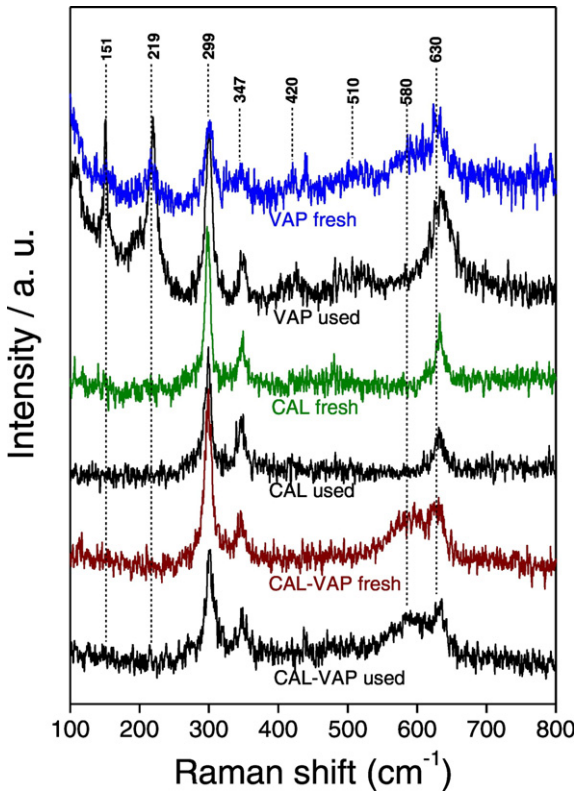

Fig. 7. LR spectra of the as synthesized and evaluated CuO_x films.

reason the Cu_4O_3 phase was not appreciated in the XRD patterns in which intense and broad peaks of CuO and Cu_2O were present (Fig. 6).

The same spectral characteristics of the fresh VAP sample is identified in the spectrum of the used VAP sample (Fig. 7), indicating that similar CuO_x species remained in this coating after being used in reaction. However, there were changes in intensities: a decrease in the signal of

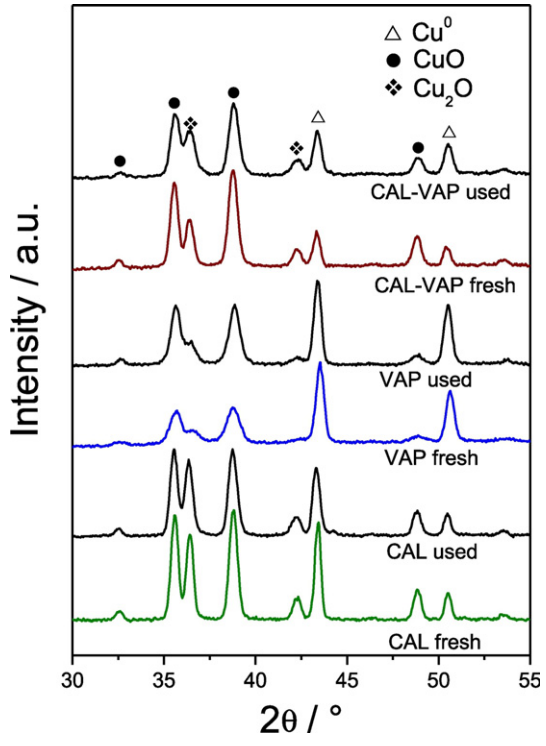

Fig. 6. XRD patterns of the as synthesized and evaluated CuO_x films.

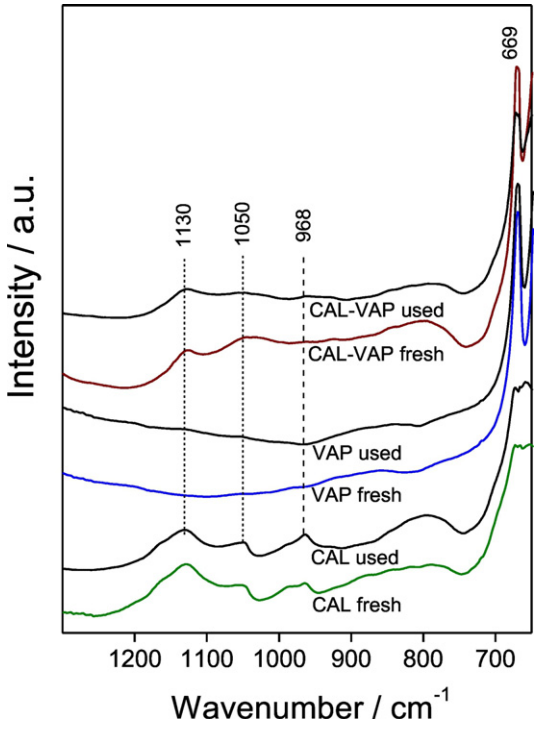

Fig. 8. DRIFT spectra of the as synthesized and evaluated samples.

Cu_4O_3 (580 cm^{-1}) was observed simultaneously with an increase in the signals of Cu_2O (151, 219, 420, 510 and 630 cm^{-1}), suggesting the reduction of the former species during the reaction. In brief, the VAP procedure induced the formation of Cu^+ and Cu^{2+} species in the outer layer of the coating. The LR spectra of fresh and used CAL were fairly similar (compare Fig. 7) and the three signals of CuO were visualized, suggesting that the outer layers were composed mainly of Cu^{2+} species. After submitting the CAL sample to a VAP procedure (fresh CAL-VAP), part of CuO was reduced to Cu_4O_3 in view that the characteristic phonon modes were observed in the LR spectrum (Fig. 7). These same Cu species were present after the reaction (Fig. 7). The reduction of CuO during the VAP step was probably due to the presence of an excess of NH_3 during this treatment, as we reported in a previous work [20].

The DRIFT spectra of fresh and used coatings are present in Fig. 8. An only phonon mode at 669 cm^{-1} is observed in the fresh VAP spectrum which was attributed to Cu^+ from the Cu_2O nanoparticles. Although this mode for bulk Cu_2O was expected around 622 cm^{-1}, the decrease of its crystal size induced a displacement to a higher frequency [41]. On the other hand, in the CAL sample two signals at 968 and 1050 cm^{-1} were observed. These IR signals were above the fundamental modes of CuO and are characteristics of small particles of this oxide after being treated at high temperatures [42]. The third signal observed at 1130 cm^{-1} can be related to O_2^- (superoxide like oxygen bond). The IR spectrum of CAL-VAP sample displayed the phonon signals of CuO, O_2^- and one at 669 cm^{-1}. The latter one was related to Cu^+ in Cu_4O_3 species [39], in agreement with the results obtained by LRS. The spectra of the samples after being maintained under reaction are similar to those of the fresh samples, indicating that no significant changes in the physicochemical nature of the nanostructures take place during the reaction.

In this context, the outer layers of the CAL coating mainly consisted of Cu^{2+} species whereas on the surface of VAP and CAL-VAP coatings, Cu^+ and Cu^{2+} species coexisted. Therefore, the active sites were different from CAL film with respect to VAP and CAL-VAP films causing the different catalytic performance of the microreactors. It has been established that the reaction rate for CO oxidation at the temperature range used in this work decreased with the increment of copper oxidation state, Cu^+ being higher than Cu^{2+} [43]. Moreover, in the VAP and CAL-VAP samples there is a certain proportion of Cu_4O_3 species which

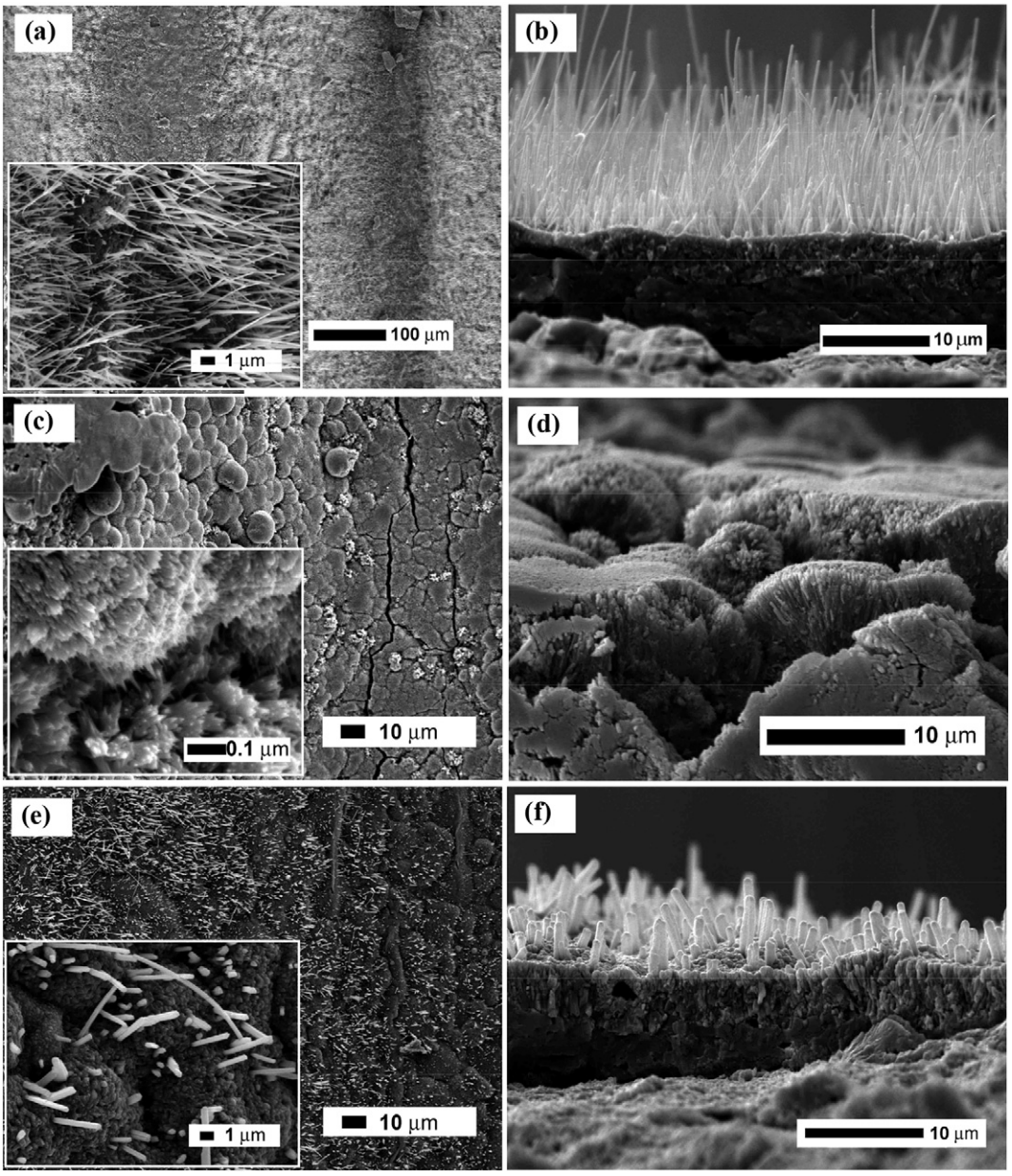

Fig. 9. SEM images of the microreactors evaluated in reaction: a–b) CAL; c–d) VAP; e–f) CAL-VAP.

have been associated with a high activity in the CO oxidation because it allows the formation of adsorbed CO_2 and O_2 species of high reactivity due to the oxygen deficiency and low-valence Cu^+ sites of this phase [44]. Furthermore, these latter films contained a higher proportion of reducible oxide species in comparison with those of the CAL film as shown by TPR (Fig. 2); thus, the higher reducibility of the active sites, the higher activity in the CO oxidation [28]. Besides, the catalytic activity tests for either VAP or CAL-VAP microreactors presented a similar behavior as shown by the curves with empty and filled symbols in Fig. 5a, respectively.

The morphological characteristics of the films after the catalytic evaluations (Fig. 9) are in line with the previous characterizations. It can be seen that the oxide nanostructures are generally maintained, although slight modifications are observed. The VAP sample retains the nanostructure of densely packed nanoribbons both on the sides and bottom of the microchannels walls (Fig. 9a, b) with nanostructures that did not change significantly their dimensions (200 nm) with respect to those of the fresh film. In the CAL sample, the needle morphology is maintained with dimensions similar to those of the fresh sample (~8.5 μm length, 270 nm width), although a smaller amount of needles is observed (Fig. 9c, d). Meanwhile, the CAL-VAP sample (Fig. 9e, f) also retained the needle morphology of the structures on the surface although these are somewhat shorter (4.5 μm) and wider (610 nm) compared to those of the fresh sample. In addition, a smaller proportion of needles was noted and small grains were observed on the film surface at the bottom of the needles (see inset in Fig. 9e), suggesting a probable transformation of the latter into nanocrystals during the catalytic use.

In brief, the catalytic performance of the CuO_x films can be comprehended through their physicochemical properties. By SEM was demonstrated that a dense surface layer of CuO_x nanostructures were produced in all the cases, favoring a good contact between the reactant stream and the catalytic surface. Considering the results obtained by XRD, FTIR and LRS it can be inferred that the crystalline phases and their proportions in each film remained the same after being under reaction for >24 h, which is also in agreement with the catalytic stability observed in reaction during that time. Besides, the analysis of LRS and DRIFT spectra pointed out that VAP films contain Cu^+ and Cu^{2+} species in the outer layer of the coating, with a certain proportion of the highly active Cu_4O_3 phase, while CAL films presents mainly Cu^{2+}. However, by submitting the CAL sample to the VAP treatment (CAL-VAP), part of CuO was reduced to Cu_2O and Cu_4O_3 species. The latter are recognized by having a higher intrinsic activity on CO oxidation than that of Cu^{2+}, therefore it can be responsible for the higher activity (lower T^{50}, and shift of the light-off temperature) of VAP and CAL-VAP microreactors. This is also in line with the TPR results, which showed that VAP and CAL-VAP films had a greater reducibility.

4. Conclusions

Homogeneous arrays of copper oxide nanostructures that totally covered the surface of copper microchannels were obtained by simple gas phase oxidation methods. VAP films had thickly clustered nanorods about 1 μm length and 150 nm width; CAL films presented a uniform growth of nanoneedles 9 μm in length and 260 nm in width, whereas CAL-VAP films presented a widening as well as a reduction in the amount of the needles. The films exhibited high mechanical stability with a level of adherence that followed the order VAP > CAL-VAP > CAL. In addition all films grown on microchannels showed a remarkable increase of the adhesion as compared to those grown on flat substrates, probably due to a better stabilization of the films onto the micro-undulated surface. The oxide layers showed a high performance for the CO oxidation reaction using a microreactor, following an activity order VAP ≈ CAL-VAP > CAL and all of them were stable under reaction conditions maintaining a high level of conversion for >24 h. The characterizations showed that the outer layers of the CAL film mainly consisted of Cu^{2+} species, whereas on the surface of VAP and CAL-VAP coatings Cu^+ and Cu^{2+} species were present. Moreover, VAP and CAL-VAP films presented a higher proportion of reducible oxides with a certain proportion of Cu_4O_3, associated with their higher catalytic activity. The CuO_x-based microreactors obtained represent a simple, low-cost alternative that shows good catalytic performance in the catalytic CO oxidation.

Acknowledgments

The authors thank the financial support received from CONICET, ANPCyT (PICT 0896) and Universidad Nacional del Litoral (CAI + D 0486) for carrying out this study. Thanks are also given to Fabio Fontanarrosa for the SEM analyses.

References

[1] S. Bennici, A. Gervasini, Catalytic activity of dispersed CuO phases towards nitrogen oxides (N_2O, NO, and NO_2), Appl. Catal. B Environ. 62 (2006) 336–344.
[2] F. Mariño, G. Baronetti, M. Laborde, N. Bion, A. Le Valant, F. Epron, D. Duprez, Optimized CuO-CeO_2 catalysts for COPROX reaction, Int. J. Hydrog. Energy 33 (2008) 1345–1353.
[3] I. López, T. Valdés-Solís, G. Marbán, An attempt to rank copper-based catalysts used in the CO-PROX reaction, Int. J. Hydrog. Energy 33 (2008) 197–205.
[4] Z. Boukha, J. Ayastuy, A. Iglesias-González, B. Pereda-Ayo, M. Gutiérrez-Ortiz, J. González-Velasco, New copper species generated on Cu/Al_2O_3-based microreactors for COPROX activity enhancement, Int. J. Hydrog. Energy 40 (2015) 7318–7328.
[5] V. Snapkauskiene, V. Valincius, P. Valatkevicius, Experimental study of catalytic CO oxidation over CuO/Al_2O_3 deposited on metal sheets, Catal. Today 176 (2011) 77–80.
[6] N. Pérez, E. Miró, J. Zamaro, Microreactors based on CuO-CeO_2/zeolite films synthesized onto brass microgrids for the oxidation of CO, Appl. Catal. B Environ. 129 (2013) 416–425.
[7] G. Kolb, V. Hessel, Micro-structured reactors for gas phase reactions, Chem. Eng. J. 98 (2004) 1–38.
[8] L. Kiwi-Minsker, A. Renken, Microstructured reactors for catalytic reactions, Catal. Today 110 (2005) 2–14.
[9] G. Groppi, G. Airoldi, C. Cristiani, E. Tronconi, Characteristics of metallic structured catalysts with high thermal conductivity, Catal. Today 60 (2000) 57–62.
[10] M. Song, S. Hwang, D. Whang, Non-enzymatic electrochemical CuO nanoflowers sensor for hydrogen peroxide detection, Talanta 80 (2010) 1648–1652.
[11] Q. Pan, H. Jin, H. Wang, G. Yin, Flower-like CuO film-electrode for lithium ion batteries and the effect of surface morphology on electrochemical performance, Electrochim. Acta 53 (2007) 951–956.
[12] Y. Liu, Y. Chu, M. Li, L. Li, L. Dong, *In situ* synthesis and assembly of copper oxide nanocrystals on copper foil *via* a mild hydrothermal process, J. Mater. Chem. 16 (2006) 192–198.
[13] A. Li, H. Song, W. Wan, J. Zhou, X. Chen, Copper oxide nanowire arrays synthesized by in-situ thermal oxidation as an anode material for lithium-ion batteries, Electrochim. Acta 132 (2014) 42–48.
[14] F. Shao, F. Hernández, J. Prades, C. Fábrega, T. Andreu, J. Morante, Copper (II) oxide nanowires for p-type conductometric NH_3 sensing, Appl. Surf. Sci. 311 (2014) 177–181.
[15] X. Jiang, T. Herricks, Y. Xia, CuO nanowires can be synthesized by heating copper substrates in air, Nano Lett. 2 (12) (2002) 1334–1338.
[16] Y. Wang, R. Shen, X. Jin, P. Zhu, Y. Ye, Y. Hu, Formation of CuO nanowires by thermal annealing copper film deposited on Ti/Si substrate, Appl. Surf. Sci. 258 (2011) 201–206.
[17] E. Filippo, M. Tepore, T. Siciliano, D. Chirizzi, C. Malitesta, R. Guascito, Room temperature facile synthesis of CuO nanostructures by resistive heating, Phys. E. 60 (2014) 59–64.
[18] M. Morales, L. Cadus, Cooper foils used as support for catalytic monoliths. Superficial nano/microstructures obtained for two treatments, Catal. Today 213 (2013) 171–182.
[19] T. Soejima, H. Yagyu, N. Kimizuka, S. Ito, One-pot alkaline vapor oxidation synthesis and electrocatalytic activity towards glucose oxidation of CuO nanobelt arrays, RCS Adv. 1 (2011) 187–190.
[20] C. Neyertz, A. Gallo, M. Ulla, J. Zamaro, Nanostructured CuO_x coatings onto cu foils: surface growth by the combination of gas-phase treatments, Surf. Coat. Technol. 285 (2016) 262–269.
[21] M. He, M. Luo, P. Fang, Characterization of CuO species and thermal solid-solid interaction in CuO/CeO_2-Al_2O_3 catalyst by in-situ XRD, Raman spectroscopy and TPR, J. Rare Earths 24 (2006) 188–192.
[22] W. Huang, Oxide nanocrystal model catalysts, Acc. Chem. Res. 49 (3) (2016) 520–527.
[23] P. Kanthale, M. Ashokkumar, F. Grieser, Experimental and theoretical investigations on sonoluminescence under dual frequency conditions, Ultrason. Sonochem. 15 (2008) 629–635.
[24] M. Lamminen, H. Walker, L. Weavers, Mechanisms and factors influencing the ultrasonic cleaning of particle-fouled ceramic membranes, J. Membr. Sci. 237 (2004) 213–223.

[25] E. Green, S. Short, IEH Assessment on Indoor Air Quality in the Home (2): Carbon Monoxide, Leicester, 1998.
[26] H. Igarashi, T. Fujino, M. Watanabe, Hydrogen electro-oxidation on platinum catalysts in the presence of trace carbon monoxide, J. Electroanal. Chem. 391 (1995) 119–123.
[27] H. Yan, X. Liu, R. Xu, P. Lv, P. Zhao, Synthesis, characterization, electrical and catalytic properties of CuO nanowires, Mater. Res. Bull. 48 (2013) 2102–2105.
[28] K. Zhou, R. Wang, B. Xu, Y. Li, Synthesis, characterization and catalytic properties of CuO nanocrystals with various shapes, Nanotechnology 17 (2006) 3939–3943.
[29] S. Salomons, R. Hayes, M. Votsmeier, A. Drochner, H. Vogel, S. Malmberg, J. Gieshoff, On the use of mechanistic CO oxidation models with a platinum monolith catalyst, Appl. Catal. B Environ. 70 (2007) 305–313.
[30] N. Pérez, E. Miró, J. Zamaro, Cu,Ce/mordenite coatings on FeCrAl-alloy corrugated foils employed as catalytic microreactors for CO oxidation, Catal. Today 213 (2013) 183–191.
[31] K. Polychronopoulou, A. Zedan, M. Katsiotis, M. Bakerd, A. AlKhoori, S. AlQaradawi, S. Hinder, S. AlHassan, Rapid microwave assisted sol-gel synthesis of CeO_2 and $Ce_xSm_{1-x}O_2$ nanoparticle catalysts for CO oxidation, J. Mol. Catal. A Chem. 428 (2017) 41–55.
[32] B. Reddy, P. Lakshmanan, P. Bharali, P. Saikia, G. Thrimurthulu, M. Muhler, W. Gru1nert, influence of alumina, silica, and titania supports on the structure and CO oxidation activity of $Ce_xZr_{1-x}O_2$ Nanocomposite oxides, J. Phys. Chem. C 111 (2007) 10478–10483.
[33] W. Liu, M. Flytzani-Stephanopoulos, Transition metal-promoted oxidation catalysis by fluorite oxides: a study of CO oxidation over Cu-CeO_2, Chem. Eng. J. 64 (1996) 283–294.
[34] C. Li, H. Yamahara, Y. Lee, H. Tabata, J. Delaunay, CuO nanowire/microflower/nanowire modified Cu electrode with enhanced electrochemical performance for non-enzymatic glucose sensing, Nanotechnology 26 (2015) 305503.
[35] A. Compaan, H. Cummins, Resonant Quadrupole-dipole Raman scattering at the 1SYellow Exciton in Cu_2O, Phys. Rev. Lett. 31 (1973) 41–43.
[36] D. Powell, A. Compaan, J. Macdonald, R. Forman, Raman-scattering study of ion-implantation-produced damage in Cu_2O, Phys. Rev. B 12 (1975) 20–25.
[37] P. Yu, Y. Shen, Resonance Raman studies in Cu_2O. I. The phonon-assisted 1s yellow excitonic absorption edge, Phys. Rev. B 12 (1975) 1377.
[38] Z. Wang, V. Pischedda, S. Saxena, P. Lazor, X-ray diffraction and Raman spectroscopic study of nanocrystalline CuO under pressures, Solid State Commun. 121 (2002) 275–279.
[39] L. Debbichi, M. Marco de Lucas, J. Pierson, P. Krüger, Vibrational properties of CuO and Cu_4O_3 from first-principles calculations, and Raman and infrared spectroscopy, J. Phys. Chem. 116 (2012) 10232–10237.
[40] J. Kim, J. Rodriguez, J. Hanson, A. Frenkel, P. Lee, Reduction of CuO and Cu_2O with H_2: H embedding and kinetic effects in the formation of suboxides, J. Am. Chem. Soc. 125 (2003) 10684–10692.
[41] D. Guo, L. Wang, Y. Du, Z. Ma, L. Shen, Preparation of octahedral Cu_2O nanoparticles by a green route, Mater. Lett. 160 (2015) 541–543.
[42] A. Davydov, Molecular Spectroscopy of Oxide Catalyst Surfaces, Wiley, New York, 2003.
[43] G. Jernigan, G. Somorjai, Carbon monoxide oxidation over three different oxidation states of copper: metallic copper, copper (I) oxide, and copper (II) oxide - a surface science and kinetic study, J. Catal. 147 (1994) 567–577.
[44] D. Svintsitskiy, T. Kardash, O. Stonkus, E. Slavinskaya, A. Stadnichenko, S. Koscheev, A. Chupakhin, A. Boronin, In situ XRD, XPS, TEM, and TPR study of highly active in CO oxidation CuO nanopowders, J. Phys. Chem. C 117 (2013) 14588–14599.